

Chameleon scalar fields in relativistic gravitational backgrounds

Shinji Tsujikawa,¹ Takashi Tamaki,^{2,3} and Reza Tavakol⁴

¹*Department of Physics, Faculty of Science, Tokyo University of Science,
1-3, Kagurazaka, Shinjuku-ku, Tokyo 162-8601, Japan**

²*Department of Physics, Waseda University, Okubo 3-4-1, Tokyo 169-8555, Japan[†]*

³*Department of Physics, Rikkyo University, Toshima, Tokyo 171-8501, Japan*

⁴*Astronomy Unit, School of Mathematical Sciences,
Queen Mary University of London, London E1 4NS, UK[‡]*

(Dated: November 5, 2018)

We study the field profile of a scalar field ϕ that couples to a matter fluid (dubbed a chameleon field) in the relativistic gravitational background of a spherically symmetric spacetime. Employing a linear expansion in terms of the gravitational potential Φ_c at the surface of a compact object with a constant density, we derive the thin-shell field profile both inside and outside the object, as well as the resulting effective coupling with matter, analytically. We also carry out numerical simulations for the class of inverse power-law potentials $V(\phi) = M^{4+n}\phi^{-n}$ by employing the information provided by our analytical solutions to set the boundary conditions around the centre of the object and show that thin-shell solutions in fact exist if the gravitational potential Φ_c is smaller than 0.3, which marginally covers the case of neutron stars. Thus the chameleon mechanism is present in the relativistic gravitational backgrounds, capable of reducing the effective coupling. Since thin-shell solutions are sensitive to the choice of boundary conditions, our analytic field profile is very helpful to provide appropriate boundary conditions for $\Phi_c \lesssim O(0.1)$.

I. INTRODUCTION

The origin of the so called dark energy responsible for the present cosmic acceleration remains a great mystery. Since the cosmological constant (originating from the vacuum energy) is plagued by a severe fine-tuning problem, many alternative models have been proposed to account for the origin of dark energy (see Refs. [1] for reviews). A number of these models, including the quintessence [2], k-essence [3] and tachyon [4] models, make use of a scalar field with a very light mass ($m_\phi \sim 10^{-33}$ eV) in order to account for the present cosmic acceleration. If the scalar field originates from candidate theories for fundamental interactions such as string theory or supergravity, it should interact with the standard model particles with a long ranged force (the so called “fifth force”). In string theory, for example, a dilaton field universally couples to matter as well as gravity [5]. Similarly, in modified gravity theories such as $f(R)$ gravity [6] and scalar-tensor theories [7], the scalar degree of freedom interacts with the matter fluid (except for radiation). This is clearly seen if one transforms the action to the Einstein frame via a conformal transformation [8]. For example, it is known that Brans-Dicke theory [9] (a historically important class of scalar-tensor theories) gives rise to a constant coupling Q between the scalar field and the matter [10]. In this sense such modified gravity theories can be regarded as a coupled quintessence scenario [11] in the Einstein frame.

In the absence of a scalar-field potential, the present solar-system tests constrain the strength of the coupling Q to be smaller than the order of 10^{-3} [10]. However, the couplings that appear in string theory [5] and $f(R)$ gravity [12] are typically of the order of unity. In such cases it is not possible to satisfy the local gravity constraints, unless a scalar-field potential with a large mass exists to suppress the coupling in the regions of high density. Moreover, if the same field is responsible for the cosmic acceleration today, the potential needs to be sufficiently flat in the regions of low density (i.e., on cosmological scales).

In spite of the above requirements it is possible for the large coupling models to satisfy the local gravity constraints through the chameleon mechanism [13, 14], while at the same time for the field to have sufficiently small mass to lead to the present cosmic acceleration. The existence of a matter coupling gives rise to an extremum of the scalar-field potential around which the field can be stabilized. In high density regions, such as the interiors of the astrophysical objects, the field mass about the extremum would be sufficiently large to avoid the propagation of the fifth force. Meanwhile, the field would have a much lighter mass in the low-density environments, far away

*Electronic address: shinji@rs.kagu.tus.ac.jp

†Electronic address: tamaki@gravity.phys.waseda.ac.jp

‡Electronic address: r.tavakol@qmul.ac.uk

from compact objects, so that it could be responsible for the present cosmic acceleration. In the case of inverse power-law potentials $V(\phi) = M^{4+n}\phi^{-n}$ [15] with $n \geq 1$, local gravity constraints can be satisfied for $M \lesssim 10^{-2}$ eV [14]. Interestingly, this roughly corresponds to the energy scale required for the cosmic acceleration today. See Refs. [16, 17, 18, 19, 20, 21, 22, 23, 24] for works concerning a number of interesting aspects of the chameleon mechanism.

So far the analyses of the chameleon mechanism have typically concentrated on the weak gravity backgrounds where the spherically symmetric metric is described by a Minkowski spacetime. This amounts to neglecting the backreaction of gravitational potential on the scalar-field equation. In Ref. [24] the field profile in the Minkowski background was analytically derived both inside and outside the object by taking into account the mass of the chameleon field inside the body. In this settings it has been shown that the field would need to be extremely close to the maximum of the effective potential around the centre of the spherically symmetric body in order to allow thin-shell solutions required for consistency with the local gravity constraints.

If we take into account the backreaction of gravitational potential to the field equation, the relativistic pressure is present even in weak gravity backgrounds such as the Sun or the Earth. It is expected that this effect changes the field profile inside the body in order to allow the existence of thin-shell solutions. We shall analytically derive the thin-shell field profile using a linear expansion in terms of the gravitational potential $\Phi_c (\ll 1)$ at the surface of compact objects. In fact we show that there exists a region around the centre of the massive objects in which the field evolves toward the maximum of the effective potential because of the presence of the relativistic pressure. In order to realize thin-shell solutions, the driving force along the potential needs to dominate over the pressure for distances larger than a critical value $r = r_3$. This distance (r_3) is required to be smaller than the distance r_1 at which the field enters a thin-shell regime. In spite of such different properties of the field profile inside the body relative to the case of the Minkowski background, the effective coupling Q_{eff} outside the body can be reduced by the presence of thin-shell solutions. We confirm this by using numerical simulations for a class of potentials of the form $V(\phi) = M^{4+n}\phi^{-n}$.

To study the viability of theories with large couplings, it is important to determine whether thin-shell solutions can also exist in strong gravitational backgrounds with $\Phi_c \lesssim \mathcal{O}(0.1)$. We shall derive analytic solutions using linear expansions in terms of Φ_c and then carry out numerical simulations to confirm the validity of solutions in the regimes with $\Phi_c \lesssim \mathcal{O}(0.1)$. Our analytic solutions are useful as a way of finding the boundary conditions around the centre of the object in order to obtain thin-shell solutions. By choosing boundary conditions with field values larger than those estimated by the analytic solutions, we shall demonstrate numerically that the thin-shell solutions are present for backgrounds with gravitational potentials satisfying $\Phi_c \lesssim 0.3$, in the case of the field potentials of the type $V(\phi) = M^{4+n}\phi^{-n}$. This marginally covers the case of neutron stars. In backgrounds with still larger gravitational potentials the relativistic pressure around the centre of the object is so strong that the field typically overshoots the maximum of the effective potential to reach the singularity at $\phi = 0$, unless the boundary conditions of the field around the centre of the body are chosen to be far from the maximum of the effective potential. This overshoot behaviour is similar to the one recently found by Kobayashi and Maeda [25] in the context of $f(R)$ dark energy models (see also Ref. [26]). We note, however, that our analytic solutions based on the linear expansion of Φ_c do not cover the field profiles for the really strong gravitational backgrounds with $\Phi_c = \mathcal{O}(1)$. In such cases we need a separate analysis which incorporates the formation of black holes.

The outline of the paper is as follows. In Section II we discuss our theoretical set up as well as giving the relevant equations for the case of a spherically symmetric central body. In section III we give the analytical thin-shell solutions to the scalar field equations, both inside and outside of the body, and consider in turn the matching of thin-shell solutions. In Section IV we study the analytical field profile in more details and discuss how the field evolves as a function of r in the presence of the relativistic pressure. In Section V we integrate the field equation numerically and show the existence of thin-shell solutions for $\Phi_c \lesssim 0.3$. Finally Section VI contains our conclusions.

II. SETUP

We consider settings in which a scalar field ϕ with potential $V(\phi)$ couples to a matter with a Lagrangian density \mathcal{L}_m . In particular we shall study theories based on the action

$$S = \int d^4x \sqrt{-g} \left[\frac{M_{\text{pl}}^2}{2} R - \frac{1}{2} (\nabla\phi)^2 - V(\phi) \right] - \int d^4x \mathcal{L}_m(\Psi_m^{(i)}, g_{\mu\nu}^{(i)}), \quad (1)$$

where g is the determinant of the metric $g_{\mu\nu}$, $M_{\text{pl}} = 1/\sqrt{8\pi G}$ is the reduced Planck mass (G is the gravitational constant), R is a Ricci scalar, and $\Psi_m^{(i)}$ are matter fields that couple to a metric $g_{\mu\nu}^{(i)}$ related with the Einstein frame metric $g_{\mu\nu}$ via

$$g_{\mu\nu}^{(i)} = e^{2Q_i\phi} g_{\mu\nu}. \quad (2)$$

Here Q_i are the strength of couplings for each matter field. In the following we shall consider cases in which the couplings are the same for each matter component, i.e., $Q_i = Q$, and use units such that $M_{\text{pl}} = 1/\sqrt{8\pi G} = 1$. We restore G when it is needed.

An example of a scalar-tensor theory which gives rise to constant couplings Q in the Einstein frame is given by the action [10]

$$\tilde{S} = \int d^4x \sqrt{-\tilde{g}} \left[\frac{1}{2} e^{-2Q\phi} \tilde{R} - \frac{1}{2} (1 - 6Q^2) e^{-2Q\phi} (\tilde{\nabla}\phi)^2 - U(\phi) \right] - \int d^4x \mathcal{L}_m(\Psi_m, \tilde{g}_{\mu\nu}), \quad (3)$$

where a tilde represents quantities in the Jordan frame. The action (3) is equivalent to that in Brans-Dicke theory with a potential $U(\phi)$. Under the conformal transformation, $g_{\mu\nu} = e^{-2Q\phi} \tilde{g}_{\mu\nu}$, we obtain the action (1) in the Einstein frame, together with the field potential $V(\phi) = U(\phi) e^{4Q\phi}$. Clearly the metric $g_{\mu\nu}^{(i)}$ in Eq. (2) corresponds to the metric $\tilde{g}_{\mu\nu}$ in the Jordan frame.

To study chameleon fields in the relativistic gravitational background of a spherically symmetric body, we consider the following spherically symmetric static metric in the Einstein frame:

$$ds^2 = -e^{2\Psi(r)} dt^2 + e^{2\Phi(r)} dr^2 + r^2 d\theta^2 + r^2 \sin^2\theta d\phi^2, \quad (4)$$

where $\Psi(r)$ and $\Phi(r)$ are functions of the distance r from the centre of symmetry. For the action (1) the energy momentum tensors for the scalar field ϕ and the matter are given, respectively, by

$$T_{\mu\nu}^{(\phi)} = \partial_\mu\phi\partial_\nu\phi - g_{\mu\nu} \left[\frac{1}{2} g^{\alpha\beta} \partial_\alpha\phi\partial_\beta\phi + V(\phi) \right], \quad (5)$$

$$T_{\mu\nu}^{(m)} = \frac{2}{\sqrt{-g}} \frac{\delta \mathcal{L}_m}{\delta g^{\mu\nu}}. \quad (6)$$

Under the gravitational background (4), the (00) and (11) components for the energy momentum tensors are

$$T_0^{0(\phi)} = -\frac{1}{2} e^{-2\Phi} \phi'^2 - V(\phi), \quad T_1^{1(\phi)} = \frac{1}{2} e^{-2\Phi} \phi'^2 - V(\phi), \quad (7)$$

where a prime represents a derivative with respect to r and

$$T_0^{0(m)} = e^{4Q\phi} \tilde{T}_0^{0(m)}, \quad T_1^{1(m)} = e^{4Q\phi} \tilde{T}_r^{r(m)}. \quad (8)$$

Here $\tilde{T}_0^{0(m)}$ and $\tilde{T}_r^{r(m)}$ are the energy momentum tensors of matter in the Jordan frame. Denoting the energy density and the pressure of the matter in the Jordan frame as $\tilde{\rho}_m$ and \tilde{p}_m , the matter energy-momentum tensor in this frame takes the form $\tilde{T}_\nu^\mu = (-\tilde{\rho}_m, \tilde{p}_m, \tilde{p}_m, \tilde{p}_m)$. The corresponding expressions for the energy density and pressure in the Einstein frame are then given by $\rho_m = e^{4Q\phi} \tilde{\rho}_m$ and $p_m = e^{4Q\phi} \tilde{p}_m$.

The evolution equation for the scalar field ϕ is given by

$$\frac{\partial}{\partial x^i} \frac{\partial(\sqrt{-g}\mathcal{L}_\phi)}{\partial(\partial\phi/\partial x^i)} - \frac{\partial(\sqrt{-g}\mathcal{L}_\phi)}{\partial\phi} - \frac{\partial\mathcal{L}_m}{\partial\phi} = 0, \quad (9)$$

where the derivative of $\mathcal{L}_m = \mathcal{L}_m(\tilde{g}_{\mu\nu}) = \mathcal{L}_m(e^{2Q\phi} g_{\mu\nu})$ in terms of ϕ is

$$\frac{\partial\mathcal{L}_m}{\partial\phi} = \sqrt{-g} Q e^{4Q\phi} \tilde{g}_{\mu\nu} \tilde{T}^{\mu\nu} = \sqrt{-g} Q (-\rho_m + 3p_m). \quad (10)$$

We then obtain

$$\phi'' + \left(\frac{2}{r} + \Psi' - \Phi' \right) \phi' = e^{2\Phi} [V_{,\phi} + Q(\rho_m - 3p_m)]. \quad (11)$$

The Einstein equations give:

$$\Phi' = \frac{1 - e^{2\Phi}}{2r} + 4\pi G r \left[\frac{1}{2} \phi'^2 + e^{2\Phi} V(\phi) + e^{2\Phi} \rho_m \right], \quad (12)$$

$$\Psi' = \frac{e^{2\Phi} - 1}{2r} + 4\pi G r \left[\frac{1}{2} \phi'^2 - e^{2\Phi} V(\phi) + e^{2\Phi} p_m \right], \quad (13)$$

$$\Psi'' + \Psi'^2 - \Psi'\Phi' + \frac{\Psi' - \Phi'}{r} = -8\pi G \left[\frac{1}{2} \phi'^2 + e^{2\Phi} V(\phi) - e^{2\Phi} p_m \right]. \quad (14)$$

From the conservation equation, $\nabla_\mu T_1^\mu = 0$, we also obtain

$$p'_m + (\rho_m + p_m)\Psi' + Q\phi'(\rho_m - 3p_m) = 0, \quad (15)$$

which is the generalization of the Tolman-Oppenheimer-Volkoff equation. Note that this equation can also be derived by combining Eqs. (11)-(14).

Our main interest is the case in which the field potential $V(\phi)$ is responsible for dark energy. In that case both $V(\phi)$ and ϕ'^2 are negligible relative to ρ_m in the local regions whose density is much larger than the cosmological one ($\rho_0 \sim 10^{-29}$ g/cm³). Then Eq. (12) can be integrated to give

$$e^{2\Phi(r)} = \left[1 - \frac{2Gm(r)}{r}\right]^{-1}, \quad m(r) = \int_0^r 4\pi r'^2 \rho_m dr'. \quad (16)$$

Substituting Eqs. (12) and (13) into Eq. (11) gives

$$\phi'' + \left[\frac{1 + e^{2\Phi}}{r} - 4\pi G r e^{2\Phi}(\rho_m - p_m)\right] \phi' = e^{2\Phi} [V_{,\phi} + Q(\rho_m - 3p_m)]. \quad (17)$$

We assume that the energy density is constant inside ($\rho_m = \rho_A$) and outside ($\rho_m = \rho_B$) of the spherically symmetric body with a radius r_c . Strictly speaking the conserved density $\rho_m^{(c)}$ in the Einstein frame is given by $\rho_m^{(c)} = e^{-Q\phi}\rho_m$ [13, 14, 24]. However, since the condition $Q\phi \ll 1$ holds in most cases of interest, we do not need to distinguish between $\rho_m^{(c)}$ and ρ_m .

Inside the spherically symmetric body ($0 < r < r_c$) we have $m(r) = 4\pi r^3 \rho_A/3$ and Eq. (16) gives

$$e^{2\Phi(r)} = \left(1 - \frac{8\pi G}{3} \rho_A r^2\right)^{-1}. \quad (18)$$

With the neglect of the scalar-field contributions in Eqs. (12)-(15) it is known that the background gravitational field for $0 < r < r_c$ corresponds to the Schwarzschild interior solution. In this case the pressure $p_m(r)$ inside the body relative to the density ρ_A can be analytically expressed as

$$\frac{p_m(r)}{\rho_A} = \frac{\sqrt{1 - 2(r^2/r_c^2)\Phi_c} - \sqrt{1 - 2\Phi_c}}{3\sqrt{1 - 2\Phi_c} - \sqrt{1 - 2(r^2/r_c^2)\Phi_c}} \quad (0 < r < r_c), \quad (19)$$

where Φ_c is the gravitational potential at the surface of body:

$$\Phi_c \equiv \frac{GM_c}{r_c} = \frac{1}{6} \rho_A r_c^2. \quad (20)$$

Here $M_c = 4\pi r_c^3 \rho_A/3$ is the mass of the spherically symmetric body, and in the last equality in Eq. (20) we have used units such that $G = 1/8\pi$. Equation (19) shows that the pressure vanishes at the surface of the body ($p_m(r_c) = 0$).

In the following we shall derive analytic solutions for Eq. (11), under the conditions $|\Phi(r)| \ll 1$ and $|\Psi(r)| \ll 1$. We neglect the terms higher than the linear order in $\Phi(r)$ and $\Psi(r)$. From Eqs. (18)-(20) it then follows that

$$\Phi(r) \simeq \Phi_c \frac{r^2}{r_c^2}, \quad \frac{p_m(r)}{\rho_A} \simeq \frac{\Phi_c}{2} \left(1 - \frac{r^2}{r_c^2}\right), \quad \text{for } 0 < r < r_c. \quad (21)$$

At the centre of the body we have $p_m(0)/\rho_A \simeq \Phi_c/2$, which shows that the effect of the pressure becomes important in strong gravitational backgrounds.

Outside the body we assume that the density ρ_B is very much smaller than ρ_A with a vanishing pressure. Then the metric outside the body can be approximated by the Schwarzschild exterior solution:

$$\Phi(r) \simeq \frac{GM}{r} = \Phi_c \frac{r_c}{r}, \quad p_m(r) \simeq 0 \quad \text{for } r > r_c. \quad (22)$$

III. MATCHING SOLUTIONS OF THE CHAMELEON SCALAR FIELD

In this section we solve the scalar-field equation (17) in the relativistic gravitational backgrounds discussed in Sec. II.

In the nonrelativistic gravitational background where the pressure p_m as well as the gravitational potential Φ_c are negligible, the effective potential for the scalar field is defined as [13, 14]

$$V_{\text{eff}}(\phi) = V(\phi) + Q\rho_m\phi. \quad (23)$$

This potential has a minimum either when (i) $V_{,\phi} < 0$ and $Q > 0$ or (ii) $V_{,\phi} > 0$ and $Q < 0$. An example of class of potentials satisfying (i) is provided by the inverse power-law potentials $V(\phi) = M^{4+n}\phi^{-n}$ ($n > 0$). Since $f(R)$ gravity corresponds to the coupling $Q = -1/\sqrt{6}$, the effective potential V_{eff} has a minimum for the case $V_{,\phi} > 0$ (as in the case of the models proposed in Refs. [27, 28, 29, 30, 31, 32]).

For constant matter densities, ρ_A and ρ_B , inside and outside of the body, the effective potential (23) has two minima at the field values ϕ_A and ϕ_B characterized by the conditions

$$V_{,\phi}(\phi_A) + Q\rho_A = 0, \quad (24)$$

$$V_{,\phi}(\phi_B) + Q\rho_B = 0. \quad (25)$$

The former corresponds to the region with a high density (interior of the body) that gives rise to a heavy mass squared $m_A^2 \equiv \frac{d^2 V_{\text{eff}}}{d\phi^2}(\phi_A)$, whereas the latter corresponds to the lower density region (exterior of the body) with a lighter mass squared $m_B^2 \equiv \frac{d^2 V_{\text{eff}}}{d\phi^2}(\phi_B)$.

The following boundary conditions are imposed at $r = 0$ and $r \rightarrow \infty$:

$$\frac{d\phi}{dr}(r = 0) = 0, \quad \phi(r \rightarrow \infty) = \phi_B. \quad (26)$$

We need to consider the potential ($-V_{\text{eff}}$) in order to find the ‘‘dynamics’’ of ϕ with respect to r . This means that the effective potential ($-V_{\text{eff}}$) has a maximum at $\phi = \phi_A$. The field ϕ is at rest at $r = 0$ and begins to roll down the potential when the matter-coupling term $Q\rho_A$ becomes important at a radius r_1 . If the field value at $r = 0$ is close to ϕ_A , the field stays around ϕ_A in the region $0 < r < r_1$. The body has a thin-shell if r_1 is close to the radius r_c of the body.

The position of the minimum given in Eq. (24) is shifted in the relativistic gravitational background. In the following we shall derive the field profile by taking into account the corrections coming from the gravitational potential. Inside the body, Eq. (17) to the linear order in Φ_c reduces to:

$$\phi'' + \frac{2}{r} \left(1 - \frac{r^2}{2r_c^2} \Phi_c\right) \phi' - (V_{,\phi} + Q\rho_A) \left(1 + 2\Phi_c \frac{r^2}{r_c^2}\right) + \frac{3}{2} Q\rho_A \Phi_c \left(1 - \frac{r^2}{r_c^2}\right) = 0. \quad (27)$$

In the region $0 < r < r_1$ the field derivative of the effective potential around $\phi = \phi_A$ may be approximated by $dV_{\text{eff}}/d\phi = V_{,\phi} + Q\rho_A \simeq m_A^2(\phi - \phi_A)$. The solution to Eq. (27) can be obtained by writing the field as $\phi = \phi_0 + \delta\phi$, where ϕ_0 is the solution in the Minkowski background and $\delta\phi$ is the perturbation induced by Φ_c . At the linear order in $\delta\phi$ and Φ_c we obtain

$$\phi_0'' + \frac{2}{r} \phi_0' - m_A^2(\phi_0 - \phi_A) = 0, \quad (28)$$

$$\delta\phi'' + \frac{2}{r} \delta\phi' - m_A^2 \delta\phi = \Phi_c \left[\frac{2m_A^2 r^2}{r_c^2} (\phi_0 - \phi_A) + \frac{r}{r_c^2} \phi_0' - \frac{3}{2} Q\rho_A \left(1 - \frac{r^2}{r_c^2}\right) \right]. \quad (29)$$

The solution to Eq. (28) that is regular at $r = 0$ is given by $\phi_0(r) = \phi_A + A(e^{-m_A r} - e^{m_A r})/r$, where A is a constant. Substituting this solution into Eq. (29) we obtain the following solution for $\phi(r)$:

$$\begin{aligned} \phi(r) = & \phi_A + \frac{A(e^{-m_A r} - e^{m_A r})}{r} \\ & - \frac{A\Phi_c}{m_A r_c^2} \left[\left(\frac{1}{3} m_A^2 r^2 - \frac{1}{4} m_A r - \frac{1}{4} + \frac{1}{8m_A r} \right) e^{m_A r} + \left(\frac{1}{3} m_A^2 r^2 + \frac{1}{4} m_A r - \frac{1}{4} - \frac{1}{8m_A r} \right) e^{-m_A r} \right] \\ & - \frac{3Q\rho_A \Phi_c}{2m_A^4 r_c^2} [m_A^2 (r^2 - r_c^2) + 6], \quad (0 < r < r_1). \end{aligned} \quad (30)$$

One can easily show that this solution satisfies the first of the boundary conditions (26).

In the region $r_1 < r < r_c$ the field $|\phi(r)|$ evolves towards larger values with increasing r . Since $|V_{,\phi}| \ll |Q\rho_A|$ in this regime one has $dV_{\text{eff}}/d\phi \simeq Q\rho_A$. In this case ϕ_0 and $\delta\phi$ satisfy

$$\phi_0'' + \frac{2}{r} \phi_0' - Q\rho_A = 0, \quad (31)$$

$$\delta\phi'' + \frac{2}{r} \delta\phi' = \Phi_c \left[\frac{r}{r_c^2} \phi_0' - \frac{1}{2} Q\rho_A \left(3 - 7 \frac{r^2}{r_c^2} \right) \right]. \quad (32)$$

We then find the following solution

$$\phi(r) = -\frac{B}{r} \left(1 - \Phi_c \frac{r^2}{2r_c^2}\right) + C + \frac{1}{6} Q \rho_A r^2 \left(1 - \frac{3}{2} \Phi_c + \frac{23}{20} \Phi_c \frac{r^2}{r_c^2}\right), \quad (r_1 < r < r_c), \quad (33)$$

where B and C are constants.

The field acquires sufficient kinetic energy in the thin-shell regime, in order to allow it to climb up the potential hill towards larger absolute values in the region outside the body. As long as the kinetic energy of the field dominates over its potential energy, the right hand side of Eq. (17) can be neglected relative to its left hand side. Also the term that includes ρ_m and p_m in the square bracket on the left hand side of Eq. (17) can be neglected relative to the term $(1 + e^{2\Phi})/r$. Using Eq. (22), the field equation reduces to

$$\phi'' + \frac{2}{r} \left(1 + \frac{GM}{r}\right) \phi' \simeq 0. \quad (34)$$

The solution to this equation is

$$\phi(r) = \phi_B + \frac{D}{r} \left(1 + \frac{GM}{r}\right) \quad (r > r_c), \quad (35)$$

where D is a constant. Note that here we have used the second boundary condition in Eq. (26).

Having obtained the solutions (30), (33) and (35) in the three regions inside and outside the central body, we proceed to match these solutions at $r = r_1$ and $r = r_c$. The thin-shell corresponds to the region defined by

$$\Delta r_c \equiv r_c - r_1 \ll r_c, \quad (36)$$

namely $\Delta r_c/r_c \ll 1$.

It is possible to satisfy the local gravity constraints as long as the field inside the body is sufficiently massive, i.e., $m_A r_c \gg 1$ (or $m_A r_1 \gg 1$). For example, in the case of the Earth with the class of potentials $V(\phi) = M^{4+n} \phi^{-n}$, we have the constraints $m_A r_c \gtrsim 10^9$, for $n = 1$, and $m_A r_c \gtrsim 10^7$, for $n = 2$, from the experimental tests of the equivalence principle [24]. Since the mass m_A becomes larger in higher density regions, the quantity $m_A r_c$ inside a strong gravitational body becomes even larger than in the case of the Sun or the Earth. We use the approximation that $e^{-m_A r_1}$ is negligible relative to $e^{m_A r_1}$ in Eq. (30).

We recall that $\Phi_c = \mathcal{O}(10^{-2})$ - $\mathcal{O}(10^{-1})$ for neutron stars, $\Phi_c = \mathcal{O}(10^{-4})$ - $\mathcal{O}(10^{-2})$ for white dwarfs, $\Phi_c = \mathcal{O}(10^{-6})$ for the Sun and $\Phi_c = \mathcal{O}(10^{-9})$ for the Earth. In the following we shall use linear expansions in terms of the three parameters $\Delta r_c/r_c$, Φ_c and $1/(m_A r_c)$ (or $1/(m_A r_1)$). We drop terms of higher order in these parameters relative to 1. We caution that our approximation loses its accuracy under the really strong gravitational backgrounds with $\Phi_c \gtrsim \mathcal{O}(0.1)$.

Using the continuity of $\phi(r)$ and $\phi'(r)$ at $r = r_1$ and $r = r_c$ we obtain

$$A \frac{e^{m_A r_1}}{r_1} \left[1 + \frac{m_A r_1^3 \Phi_c}{3r_c^2} \left(1 - \frac{3}{4m_A r_1}\right)\right] - B \frac{1}{r_1} \left(1 - \Phi_c \frac{r_1^2}{2r_c^2}\right) + C = \phi_A - \frac{Q \rho_A r_1^2}{6} \left(1 - \frac{3}{2} \Phi_c + \frac{23}{20} \Phi_c \frac{r_1^2}{r_c^2}\right), \quad (37)$$

$$A \frac{m_A e^{m_A r_1}}{r_1} \left[1 + \frac{m_A r_1^3 \Phi_c}{3r_c^2} \left(1 + \frac{5}{4m_A r_1}\right) - \frac{1}{m_A r_1}\right] + B \frac{1}{r_1^2} \left(1 + \Phi_c \frac{r_1^2}{2r_c^2}\right) = -\frac{1}{6} Q \rho_A r_1 \left(2 - 3\Phi_c + \frac{23}{5} \Phi_c \frac{r_1^2}{r_c^2}\right), \quad (38)$$

$$B \frac{1}{r_c} \left(1 - \frac{\Phi_c}{2}\right) - C + D \frac{1}{r_c} (1 + \Phi_c) = -\phi_B + \frac{1}{6} Q \rho_A r_c^2 \left(1 - \frac{7}{20} \Phi_c\right), \quad (39)$$

$$B \left(1 + \frac{\Phi_c}{2}\right) + D(1 + 2\Phi_c) = -\frac{1}{6} Q \rho_A r_c^3 \left(2 + \frac{8}{5} \Phi_c\right). \quad (40)$$

The value of C can be derived from Eqs. (39) and (40) keeping terms to linear order in Φ_c only. Substituting C into Eq. (37) and using Eq. (38) we can obtain expressions for A and B . The coefficient D is then obtained from

Eq. (40). Using this procedure we find

$$A = \frac{1}{m_A e^{m_A r_1}} \left[1 + \Phi_c \frac{r_1^2}{4r_c^2} + \frac{m_A r_1^3 \Phi_c}{3r_c^2} \left(1 - \Phi_c \frac{r_1^2}{2r_c^2} \right) \right]^{-1} \left[(\phi_A - \phi_B) \left(1 + \Phi_c \frac{r_1^2}{2r_c^2} \right) + \frac{1}{2} Q \rho_A r_c^2 \left(1 - \frac{\Phi_c}{4} + \Phi_c \frac{r_1^2}{2r_c^2} \right) - \frac{1}{2} Q \rho_A r_1^2 \left(1 - \frac{3}{2} \Phi_c + \frac{7}{4} \Phi_c \frac{r_1^2}{r_c^2} \right) \right], \quad (41)$$

$$B = -(1 - \alpha) r_1 \left[(\phi_A - \phi_B) \left(1 + \Phi_c \frac{r_1^2}{2r_c^2} \right) + \frac{1}{2} Q \rho_A r_c^2 \left(1 - \frac{\Phi_c}{4} + \Phi_c \frac{r_1^2}{2r_c^2} \right) - \frac{1}{2} Q \rho_A r_1^2 \left(1 - \frac{3}{2} \Phi_c + \frac{7}{4} \Phi_c \frac{r_1^2}{r_c^2} \right) \right] - \frac{1}{3} Q \rho_A r_1^3 \left(1 - \frac{3}{2} \Phi_c + \frac{9}{5} \Phi_c \frac{r_1^2}{r_c^2} \right), \quad (42)$$

$$C = \phi_B - \frac{1}{2} Q \rho_A r_c^2 \left(1 - \frac{\Phi_c}{4} \right), \quad (43)$$

$$D = (1 - \alpha) r_1 \left[(\phi_A - \phi_B) \left(1 + \Phi_c \frac{r_1^2}{2r_c^2} - \frac{3}{2} \Phi_c \right) + \frac{1}{2} Q \rho_A r_c^2 \left(1 - \frac{7}{4} \Phi_c + \Phi_c \frac{r_1^2}{2r_c^2} \right) - \frac{1}{2} Q \rho_A r_1^2 \left(1 - 3\Phi_c + \frac{7}{4} \Phi_c \frac{r_1^2}{r_c^2} \right) \right] - \frac{1}{3} Q \rho_A r_c^3 \left(1 - \frac{6}{5} \Phi_c \right) + \frac{1}{3} Q \rho_A r_1^3 \left(1 - 3\Phi_c + \frac{9}{5} \Phi_c \frac{r_1^2}{r_c^2} \right), \quad (44)$$

where

$$\alpha \equiv \frac{(r_1^2/3r_c^2)\Phi_c + 1/(m_A r_1)}{1 + (r_1^2/4r_c^2)\Phi_c + (m_A r_1^3 \Phi_c/3r_c^2)(1 - (r_1^2/2r_c^2)\Phi_c)}. \quad (45)$$

Since the denominator in Eq. (45) is larger than 1, the parameter α is much smaller than 1.

The distance r_1 is determined by the condition

$$m_A^2 [\phi(r_1) - \phi_A] = Q \rho_A, \quad (46)$$

where

$$\phi(r_1) = \phi_A - A \frac{e^{m_A r_1}}{r_1} \left[1 + \frac{m_A r_1^3 \Phi_c}{3r_c^2} \left(1 - \frac{3}{4m_A r_1} \right) \right] - \frac{3Q \rho_A \Phi_c}{2m_A^4 r_c^2} [m_A^2 (r_1^2 - r_c^2) + 6]. \quad (47)$$

Substituting Eq. (47) into Eq. (46) gives

$$A = -\frac{Q \rho_A r_1}{m_A^2 e^{m_A r_1}} \left(1 + \frac{m_A r_1^3 \Phi_c}{3r_c^2} - \frac{\Phi_c r_1^2}{4 r_c^2} \right)^{-1}. \quad (48)$$

From Eqs. (41) and (48) we then obtain

$$\phi_A - \phi_B = -Q \rho_A r_c^2 \left[\frac{\Delta r_c}{r_c} \left(1 + \Phi_c - \frac{1}{2} \frac{\Delta r_c}{r_c} \right) + \frac{1}{m_A r_c} \left(1 - \frac{\Delta r_c}{r_c} \right) (1 - \beta) \right], \quad (49)$$

where

$$\beta \equiv \frac{(m_A r_1^3 \Phi_c/3r_c^2)(r_1^2/r_c^2)\Phi_c}{1 + (m_A r_1^3 \Phi_c/3r_c^2) - (r_1^2/4r_c^2)\Phi_c}. \quad (50)$$

Note that $\beta \ll 1$.

The thin-shell parameter introduced in Refs. [13, 14] is in this case given by

$$\epsilon_{\text{th}} \equiv \frac{\phi_B - \phi_A}{6Q \Phi_c} \quad (51)$$

$$= \frac{\Delta r_c}{r_c} \left(1 + \Phi_c - \frac{1}{2} \frac{\Delta r_c}{r_c} \right) + \frac{1}{m_A r_c} \left(1 - \frac{\Delta r_c}{r_c} \right) (1 - \beta). \quad (52)$$

To the first-order in expansion parameters one has $\epsilon_{\text{th}} = \Delta r_c/r_c + 1/(m_A r_c)$, which is identical to the corresponding value derived in the Minkowski background [24]. The effect of the gravitational potential appears as a second-order term to the thin-shell parameter. Substituting Eq. (49) into Eq. (44), we obtain the following approximate solution

$$D \simeq -6Q\Phi_c r_c \left[\frac{\Delta r_c}{r_c} \left(1 - \frac{\Delta r_c}{r_c} \right) + \frac{1}{m_A r_c} \left(1 - 2\frac{\Delta r_c}{r_c} - \Phi_c - \alpha - \beta \right) \right], \quad (53)$$

where we have carried out a linear expansion in terms of α , β , $\Delta r_c/r_c$ and Φ_c . The solution outside the body is then given by

$$\phi(r) \simeq \phi_B - 2Q_{\text{eff}} \frac{GM}{r} \left(1 + \frac{GM}{r} \right), \quad (54)$$

where the effective coupling is

$$Q_{\text{eff}} = 3Q \left[\frac{\Delta r_c}{r_c} \left(1 - \frac{\Delta r_c}{r_c} \right) + \frac{1}{m_A r_c} \left(1 - 2\frac{\Delta r_c}{r_c} - \Phi_c - \alpha - \beta \right) \right]. \quad (55)$$

To leading-order this gives $Q_{\text{eff}} = 3Q(\Delta r_c/r_c + 1/m_A r_c) = 3Q\epsilon_{\text{th}}$, which agrees with the corresponding result in the Minkowski background [24]. Thus provided that $\epsilon_{\text{th}} \ll 1$, the effective coupling Q_{eff} becomes much smaller than the bare coupling Q . The gravitational potential Φ_c appears as a next-order term. As can be seen from Eq. (55) the presence of the gravitational potential Φ_c leads to a small decrease in Q_{eff} compared to the nonrelativistic gravitational background.

IV. THE FIELD PROFILE

In this section we shall discuss the analytical field profile derived in the previous section in more details. The coefficient A and the field difference $\phi_A - \phi_B$ are determined by fixing the value of r_1 , see Eqs. (48) and (49). From Eqs. (30), (33), (35), (42)-(44), (48) and (49) the thin-shell field profile is given by

$$\begin{aligned} \phi(r) = & \phi_A + \frac{Q\rho_A}{m_A^2 e^{m_A r_1}} \frac{r_1}{r} \left(1 + \frac{m_A r_1^3 \Phi_c}{3r_c^2} - \frac{\Phi_c r_1^2}{4r_c^2} \right)^{-1} (e^{m_A r} - e^{-m_A r}) + \frac{3Q\rho_A \Phi_c}{2m_A^2} \left[1 - \frac{r^2}{r_c^2} - \frac{6}{(m_A r_c)^2} \right] \\ & + \frac{\Phi_c r_1}{m_A r_c^2} \frac{Q\rho_A}{m_A^2 e^{m_A r_1}} \left(1 + \frac{m_A r_1^3 \Phi_c}{3r_c^2} - \frac{\Phi_c r_1^2}{4r_c^2} \right)^{-1} \\ & \times \left[\left(\frac{1}{3} m_A^2 r^2 - \frac{1}{4} m_A r - \frac{1}{4} + \frac{1}{8m_A r} \right) e^{m_A r} + \left(\frac{1}{3} m_A^2 r^2 + \frac{1}{4} m_A r - \frac{1}{4} - \frac{1}{8m_A r} \right) e^{-m_A r} \right] \quad (0 < r < r_1), \end{aligned} \quad (56)$$

$$\phi(r) = \phi_A + \frac{Q\rho_A r_c^2}{6} \left[6\epsilon_{\text{th}} + 6\tilde{B} \frac{r_1}{r} \left(1 - \frac{\Phi_c r^2}{2r_c^2} \right) - 3 \left(1 - \frac{\Phi_c}{4} \right) + \left(\frac{r}{r_c} \right)^2 \left(1 - \frac{3}{2}\Phi_c + \frac{23\Phi_c r^2}{20r_c^2} \right) \right] \quad (r_1 < r < r_c), \quad (57)$$

$$\phi(r) = \phi_A + Q\rho_A r_c^2 \left[\epsilon_{\text{th}} - \tilde{D} \frac{r_c}{r} \left(1 + \Phi_c \frac{r_c}{r} \right) \right] \quad (r > r_c), \quad (58)$$

where

$$\begin{aligned} \tilde{B} \equiv -\frac{B}{Q\rho_A r_c^2 r_1} = & (1 - \alpha) \left[-\epsilon_{\text{th}} \left(1 + \frac{\Phi_c r_1^2}{2r_c^2} \right) + \frac{1}{2} \left(1 - \frac{\Phi_c}{4} + \frac{\Phi_c r_1^2}{2r_c^2} \right) - \frac{r_1^2}{2r_c^2} \left(1 - \frac{3}{2}\Phi_c + \frac{7\Phi_c r_1^2}{4r_c^2} \right) \right] \\ & + \frac{r_1^2}{3r_c^2} \left(1 - \frac{3}{2}\Phi_c + \frac{9\Phi_c r_1^2}{5r_c^2} \right), \end{aligned} \quad (59)$$

$$\begin{aligned} \tilde{D} \equiv -\frac{D}{Q\rho_A r_c^3} = & (1 - \alpha) \left[\epsilon_{\text{th}} \frac{r_1}{r_c} \left(1 + \frac{\Phi_c r_1^2}{2r_c^2} - \frac{3\Phi_c}{2} \right) - \frac{r_1}{2r_c} \left(1 - \frac{7}{4}\Phi_c + \frac{\Phi_c r_1^2}{2r_c^2} \right) + \frac{r_1^3}{2r_c^3} \left(1 - 3\Phi_c + \frac{7\Phi_c r_1^2}{4r_c^2} \right) \right] \\ & + \frac{1}{3} \left(1 - \frac{6}{5}\Phi_c \right) - \frac{r_1^3}{3r_c^3} \left(1 - 3\Phi_c + \frac{9\Phi_c r_1^2}{5r_c^2} \right). \end{aligned} \quad (60)$$

Note that the field profile given in Eqs. (56)-(58) has been derived without specifying the form of the potential. While the term ρ_A in Eqs. (56)-(58) can be replaced by $6\Phi_c/r_c^2$, we have chosen not to do this so that the field profile in the Minkowski background can be simply recovered by setting $\Phi_c = 0$.

In the following we shall consider in details the field profile in three regions: (i) $0 < r < r_2 \equiv 1/m_A$, (ii) $r_2 < r < r_1$ and (iii) $r > r_1$, and discuss the case $Q > 0$ for simplicity.

A. The region $0 < r < r_2$

Deep inside the body where the distance r satisfies the condition $r \ll 1/m_A$, Eq. (56) gives the following approximate field value and its derivative with respect to r :

$$\phi(r) \simeq \phi_A + \frac{2Q\rho_A r_1}{m_A e^{m_A r_1}} \left(1 + \frac{m_A r_1^3 \Phi_c}{3r_c^2} - \frac{\Phi_c r_1^2}{4r_c^2} \right)^{-1} \left[1 + \frac{1}{6}(m_A r)^2 + \frac{\Phi_c}{2(m_A r_c)^2} \right] + \frac{3Q\rho_A \Phi_c}{2m_A^2} \left[1 - \frac{r^2}{r_c^2} - \frac{6}{(m_A r_c)^2} \right], \quad (61)$$

$$\phi'(r) \simeq Q\rho_A r_c^2 \left[\frac{2m_A r_1}{3e^{m_A r_1}} \left(1 + \frac{m_A r_1^3 \Phi_c}{3r_c^2} - \frac{\Phi_c r_1^2}{4r_c^2} \right)^{-1} - \frac{3\Phi_c}{(m_A r_c)^2} \right] \frac{r}{r_c^2}. \quad (62)$$

In the Minkowski background ($\Phi_c = 0$) we have $\phi(0) \simeq \phi_A + 2Q\rho_A r_1/(m_A e^{m_A r_1})$ and $\phi'(r) > 0$ (where $r \neq 0$). Hence the field rolls down the potential toward larger ϕ with increasing r . In the presence of the gravitational potential Φ_c , the derivative $\phi'(r)$ can be negative depending on model parameters. Using the approximation $r_c \simeq r_1$ the condition that $\phi'(r) < 0$ translates into

$$\frac{(m_A r_1)^3}{e^{m_A r_1}} - \frac{3}{2}\Phi_c^2 m_A r_1 < \frac{9}{2}\Phi_c \left(1 - \frac{\Phi_c}{4} \right). \quad (63)$$

When $\Phi_c > 0.253$ this is automatically satisfied for all (positive) $m_A r_1$. When $\Phi_c = 10^{-1}, 10^{-6}, 10^{-9}$, the condition (63) is satisfied for $m_A r_1 > 6$, $m_A r_1 > 22$ and $m_A r_1 > 29$, respectively. Hence in most realistic cases where $m_A r_1 \gg 1$ we have $\phi'(r) < 0$ in the region $0 < r < r_2$. Interestingly this property persists even in the weak gravitational backgrounds, such as those of the Sun or the Earth.

The evolution towards the smaller ϕ region is due to the effects of the relativistic pressure p_m since the last term on the right hand side of Eq. (61) originates from the pressure. Compared to the case of the Minkowski spacetime, the presence of the pressure term leads to the shift of the field $\phi(0)$ towards a larger value. When this effect of the pressure dominates over the rolling down effect along the potential, we have

$$\phi(r) \simeq \phi_A + \frac{3Q\rho_A \Phi_c}{2m_A^2} \left[1 - \frac{r^2}{r_c^2} - \frac{6}{(m_A r_c)^2} \right]. \quad (64)$$

This shows that the field decreases from $\phi(0) \simeq \phi_A + \frac{3Q\rho_A \Phi_c}{2m_A^2} [1 - 6/(m_A r_c)^2]$ to $\phi(r_2) \simeq \phi_A + \frac{3Q\rho_A \Phi_c}{2m_A^2} [1 - 7/(m_A r_c)^2]$ with increasing r .

B. The region $r_2 < r < r_1$

In the region $r_2 < r < r_1$ we have the following approximate solutions from Eq. (56):

$$\phi(r) \simeq \phi_A + \frac{Q\rho_A}{m_A^2} e^{m_A(r-r_1)} \frac{r_1/r + m_A \Phi_c r_1 r^2 / 3r_c^2 - \Phi_c r_1 r / 4r_c^2}{1 + m_A r_1^3 \Phi_c / 3r_c^2 - \Phi_c r_1^2 / 4r_c^2} + \frac{3Q\rho_A \Phi_c}{2m_A^2} \left[1 - \frac{r^2}{r_c^2} - \frac{6}{(m_A r_c)^2} \right], \quad (65)$$

$$\begin{aligned} \phi'(r) &\simeq \frac{Q\rho_A}{m_A^2} \left(1 + \frac{m_A r_1^3 \Phi_c}{3r_c^2} - \frac{\Phi_c r_1^2}{4r_c^2} \right)^{-1} m_A e^{m_A(r-r_1)} \\ &\times \left[\frac{r_1}{r} + \frac{\Phi_c m_A r_1 r^2}{3r_c^2} - \frac{\Phi_c r_1 r}{4r_c^2} - \frac{1}{m_A r} \left(\frac{r_1}{r} - \frac{2\Phi_c m_A r_1 r^2}{3r_c^2} + \frac{\Phi_c r_1 r}{4r_c^2} \right) \right] - \frac{3Q\rho_A \Phi_c}{(m_A r_c)^2} r. \end{aligned} \quad (66)$$

In Eq. (65) we have taken into account the terms $(m_A^2 r^2 / 3 - m_A r / 4) e^{m_A r}$ in the last square bracket of Eq. (56). If $\phi'(r) < 0$ at $r = r_2$, the field derivative needs to change its sign from negative to positive at the distance r_3 (i.e., $\phi'(r_3) = 0$).

From Eq. (66) the condition $\phi'(r_3) = 0$ translates to

$$\begin{aligned} &m_A r_c e^{m_A(r_3-r_1)} \left[\frac{r_1}{r_3} + \frac{\Phi_c m_A r_1 r_3^2}{3r_c^2} - \frac{\Phi_c r_1 r_3}{4r_c^2} - \frac{1}{m_A r_3} \left(\frac{r_1}{r_3} - \frac{2\Phi_c m_A r_1 r_3^2}{3r_c^2} + \frac{\Phi_c r_1 r_3}{4r_c^2} \right) \right] \\ &= 3\Phi_c \frac{r_3}{r_c} \left(1 + \frac{m_A r_1^3 \Phi_c}{3r_c^2} - \frac{\Phi_c r_1^2}{4r_c^2} \right). \end{aligned} \quad (67)$$

	$m_{Ar_1} = 10$	$m_{Ar_1} = 10^2$	$m_{Ar_1} = 10^3$
$\Phi_c = 10^{-9}$	$\phi'(r) > 0$	0.75	0.97
$\Phi_c = 10^{-6}$	$\phi'(r) > 0$	0.82	0.98
$\Phi_c = 10^{-1}$	0.55	0.94	0.99

Table I: The values of r_3/r_1 at which $\phi'(r_3) = 0$ under the approximation $r_c \simeq r_1$. It is clear that r_3/r_1 increases for larger Φ_c and m_{Ar_1} . In the cases $\Phi_c = 10^{-9}$ and $\Phi_c = 10^{-6}$ with $m_{Ar_1} = 10$ the field derivatives $\phi'(r)$ are positive in the region $1/m_A < r < r_1$.

In Table I we show the values of r_3/r_1 under the approximation $r_c \simeq r_1$ for several different choices of Φ_c and m_{Ar_1} . Clearly r_3/r_1 gets larger with increasing Φ_c and m_{Ar_1} . When $\Phi_c = 10^{-6}$ and $\Phi_c = 10^{-9}$ with $m_{Ar_1} = 10$ the field satisfies the condition $\phi'(r) > 0$ in the region $r_2 < r < r_1$. Meanwhile, when $\Phi_c = 10^{-1}$ and $m_{Ar_1} = 10$, the sign change of $\phi'(r)$ occurs at $r_3/r_1 = 0.55$.

In the region $r \gtrsim r_3$ the second term on the right hand side of Eq. (65) dominates over the third one, giving the following solution

$$\phi(r) \simeq \phi_A + \frac{Q\rho_A}{m_A^2} e^{m_A(r-r_1)} \frac{r_1/r + m_A\Phi_c r_1 r^2/3r_c^2 - \Phi_c r_1 r/4r_c^2}{1 + m_{Ar_1}^3 \Phi_c/3r_c^2 - \Phi_c r_1^2/4r_c^2}. \quad (68)$$

At $r = r_1$ we have $\phi(r_1) = \phi_A + Q\rho_A/m_A^2$, as required by Eq. (46). Note that $|\phi(r_1) - \phi_A|$ is larger than $|\phi(0) - \phi_A|$ by a factor of $2/(3\Phi_c)$.

C. The region $r > r_1$

In the region $r_1 < r < r_c$ the field ϕ grows because of the dominance of the last term in Eq. (57). The field value at the surface of the body can be estimated as

$$\phi(r_c) \simeq \phi_A + Q\rho_{Ar_c}^2 \left[\frac{1}{m_{Ar_c}} \alpha + \frac{1}{2} \left(\frac{\Delta r_c}{r_c} \right)^2 + \frac{1}{m_{Ar_c}} \frac{\Delta r_c}{r_c} \right] \simeq \phi_A + \frac{Q\rho_A}{m_A^2} \left[1 + \frac{1}{2} \left(m_{Ar_c} \frac{\Delta r_c}{r_c} \right)^2 + m_{Ar_c} \frac{\Delta r_c}{r_c} \right], \quad (69)$$

where in the second approximate equality we have used the fact that α is of the order of $1/(m_{Ar_1})$. Obviously $\phi(r_c)$ is larger than $\phi(r_1)$. If the condition

$$\frac{\Delta r_c}{r_c} \gg \frac{1}{m_{Ar_c}}, \quad (70)$$

is satisfied, we have that $\phi(r_c) \gg \phi(r_1)$. In this case the field acquires a sufficient amount of kinetic energy so that the following condition is satisfied at $r = r_c$:

$$\phi'' + \frac{2}{r} \phi' \simeq Q\rho_A \gg |V_{,\phi}|. \quad (71)$$

We recall that outside the body the density ρ_A sharply drops down to ρ_B . Hence only the potential-dependent term remains on the right hand side of Eq. (17). Under the condition (71) the kinetic energy dominates over $|V_{,\phi}|$ for $r > r_c$ so that the field equation is approximately given by Eq. (34). In this case the analytic field profile should be trustworthy.

If the condition (70) is not satisfied, the field $\phi(r_c)$ is not much different from $\phi(r_1)$. In this case the kinetic energy of the field is not sufficiently large so that the term $|V_{,\phi}|$ is not negligible relative to $Q\rho_A$ at $r = r_c$. In the region $r > r_c$, this can lead to the pullback of the field because the kinetic energy is not large enough for the field to climb up the potential hill. In fact we have numerically confirmed this behaviour in cases where $\Delta r_c/r_c$ is smaller than the order of $1/(m_{Ar_c})$. Thus the condition (70) is important in order to obtain the field solution (35) outside the body.

V. NUMERICAL SIMULATIONS

In this section we shall numerically confirm the analytic field profile presented in the previous section and discuss the validity of the approximations used to derive it. In these numerical simulations we employ the class of inverse power-law potentials

$$V(\phi) = M^{4+n} \phi^{-n} \quad (n > 0). \quad (72)$$

Although we specify the field potential to be of the form (72), the thin-shell field profile we will derive numerically in this section also holds for other potentials, such as $V(\phi) = M^4 \exp(M^n/\phi^n)$, as can be expected from the general form of the Eqs. (56)-(58). The effective potential V_{eff} has extrema inside and outside the body for $Q > 0$. The field value ϕ_A and the mass squared m_A^2 inside the body are given by

$$\phi_A = \left[\frac{n M^{4+n}}{Q \rho_A} \right]^{1/(n+1)}, \quad m_A^2 = n(n+1) \left(\rho_A \frac{Q}{n} \right)^{(n+2)/(n+1)} M^{-(n+4)/(n+1)}, \quad (73)$$

which lead to the following relation

$$\phi_A = \frac{(n+1)Q\rho_A r_c^2}{(m_A r_c)^2}. \quad (74)$$

The field value ϕ_B and the mass m_B can be obtained by replacing ρ_A for ρ_B in Eq. (73).

We introduce a dimensionless field φ defined by

$$\varphi \equiv \phi/\phi_A. \quad (75)$$

From Eqs. (56)-(58) the analytic thin-shell field profile for the potential (72) is given by

$$\begin{aligned} \varphi(r) = & 1 + \frac{1}{(n+1)e^{m_A r_1}} \frac{r_1}{r} \left(1 + \frac{m_A r_1^3 \Phi_c}{3r_c^2} - \frac{\Phi_c r_1^2}{4r_c^2} \right)^{-1} (e^{m_A r} - e^{-m_A r}) + \frac{3\Phi_c}{2(n+1)} \left[1 - \frac{r^2}{r_c^2} - \frac{6}{(m_A r_c)^2} \right] \\ & + \frac{\Phi_c}{(n+1)e^{m_A r_1}} \frac{r_1}{m_A r_c^2} \left(1 + \frac{m_A r_1^3 \Phi_c}{3r_c^2} - \frac{\Phi_c r_1^2}{4r_c^2} \right)^{-1} \\ & \times \left[\left(\frac{1}{3} m_A^2 r^2 - \frac{1}{4} m_A r - \frac{1}{4} + \frac{1}{8m_A r} \right) e^{m_A r} + \left(\frac{1}{3} m_A^2 r^2 + \frac{1}{4} m_A r - \frac{1}{4} - \frac{1}{8m_A r} \right) e^{-m_A r} \right] \quad (0 < r < r_1), \end{aligned} \quad (76)$$

$$\varphi(r) = 1 + \frac{(m_A r_c)^2}{n+1} \left[\epsilon_{\text{th}} + \tilde{B} \frac{r_1}{r} \left(1 - \frac{\Phi_c r^2}{2r_c^2} \right) - \frac{1}{2} \left(1 - \frac{1}{4} \Phi_c \right) + \frac{1}{6} \left(\frac{r}{r_c} \right)^2 \left(1 - \frac{3}{2} \Phi_c + \frac{23\Phi_c r^2}{20r_c^2} \right) \right] \quad (r_1 < r < r_c), \quad (77)$$

$$\varphi(r) = 1 + \frac{(m_A r_c)^2}{n+1} \left[\epsilon_{\text{th}} - \tilde{D} \frac{r_c}{r} \left(1 + \Phi_c \frac{r_c}{r} \right) \right] \quad (r > r_c). \quad (78)$$

Introducing a dimensionless distance normalized by r_c :

$$x \equiv r/r_c, \quad (79)$$

the field equations to be solved numerically take the forms

$$\frac{d^2\varphi}{dx^2} + \frac{2 - 5\Phi_c x^2 + 3\Phi_c x^2 p_m/\rho_m}{x(1 - 2\Phi_c x^2)} \frac{d\varphi}{dx} = \frac{(m_A r_c)^2}{n+1} \frac{1}{1 - 2\Phi_c x^2} \left[1 - \frac{3p_m(r)}{\rho_A} - \frac{1}{\varphi^{n+1}} \right] \quad (0 < x < 1), \quad (80)$$

$$\frac{d^2\varphi}{dx^2} + \frac{2(1 - \Phi_c/x) - 3\Phi_c x^2 \rho_B/\rho_A}{x - 2\Phi_c} \frac{d\varphi}{dx} = \frac{(m_A r_c)^2}{n+1} \frac{1}{1 - 2\Phi_c/x} \left(\frac{\rho_B}{\rho_A} - \frac{1}{\varphi^{n+1}} \right) \quad (x > 1), \quad (81)$$

where $p_m(r)/\rho_A$ is given in Eq. (19). Given the occurrence of x in the denominator of the second term of Eq. (80), the numerical solutions cannot start from the centre of the body ($x = 0$). Instead we start the integrations from a radius $r = r_i$, slightly away from the centre satisfying the condition $r_i \ll 1/m_A$. In so doing we use the analytic solution (76) with the field derivative

$$\begin{aligned} \frac{d\varphi}{dx} = & \frac{1}{n+1} \left[\frac{1}{e^{m_A r_1}} \left(1 + \frac{m_A r_1^3 \Phi_c}{3r_c^2} - \frac{\Phi_c r_1^2}{4r_c^2} \right)^{-1} \frac{r_c r_1}{r^2} \left\{ m_A r (e^{-m_A r} + e^{m_A r}) + e^{-m_A r} - e^{m_A r} \right. \right. \\ & + \frac{r^2}{r_c^2} \Phi_c \left(\left(\frac{1}{3} m_A^2 r^2 + \frac{5}{12} m_A r - \frac{1}{2} + \frac{1}{8m_A r} - \frac{1}{8m_A^2 r^2} \right) e^{m_A r} \right. \\ & \left. \left. - \left(\frac{1}{3} m_A^2 r^2 - \frac{5}{12} m_A r - \frac{1}{2} - \frac{1}{8m_A r} - \frac{1}{8m_A^2 r^2} \right) e^{-m_A r} \right\} - 3\Phi_c \frac{r}{r_c} \right]. \end{aligned} \quad (82)$$

From Eq. (73) we have that $\phi_B/\phi_A = (\rho_A/\rho_B)^{1/(n+1)}$ and hence $\epsilon_{\text{th}} = (n+1)/(m_{Ar_c})^2[(\rho_A/\rho_B)^{1/(n+1)} - 1]$. Using Eq. (52) we obtain the following relation for the ratio ρ_A/ρ_B

$$\frac{\rho_A}{\rho_B} = \left[1 + \frac{(m_{Ar_c})^2}{n+1} \left\{ \frac{\Delta r_c}{r_c} \left(1 + \Phi_c - \frac{1}{2} \frac{\Delta r_c}{r_c} \right) + \frac{1}{m_{Ar_c}} \left(1 - \frac{\Delta r_c}{r_c} \right) (1 - \beta) \right\} \right]^{n+1}. \quad (83)$$

Thus specifying the values of n , m_{Ar_c} , $\Delta r_c/r_c$ and Φ_c , allows the ratio ρ_A/ρ_B to be determined. Alternatively, given the ratio ρ_A/ρ_B together with n and Φ_c , allows the relationship between m_{Ar_c} and $\Delta r_c/r_c$ to be derived. We note that the condition $\Delta r_c/r_c \gg 1/(m_{Ar_c})$ needs to be satisfied for the field to have a sufficient kinetic energy outside the body.

A. Minkowski background ($\Phi_c = 0$)

Let us first consider the Minkowski background ($\Phi_c = 0$). In this case the analytic field profile is given by

$$\varphi(x) = 1 + \frac{1}{(n+1)e^{m_{Ar_1}}} \frac{r_1}{r_c} \frac{1}{x} (e^{m_{Ar_c}x} - e^{-m_{Ar_c}x}) \quad (0 < r < r_1), \quad (84)$$

$$\varphi(x) = 1 + \frac{(m_{Ar_c})^2}{n+1} \left[\epsilon_{\text{th}} + \frac{1}{6}(x^2 - 3) + \frac{r_1^3}{3r_c^3} \frac{1}{x} - \left(1 - \frac{1}{m_{Ar_1}} \right) \frac{1}{m_{Ar_c}} \frac{r_1^2}{r_c^2} \frac{1}{x} \right] \quad (r_1 < r < r_c), \quad (85)$$

$$\varphi(x) = 1 + \frac{(m_{Ar_c})^2}{n+1} \left[\epsilon_{\text{th}} - \frac{r_1}{r_c} \frac{1}{x} \left\{ \epsilon_{\text{th}} + \frac{r_c}{6r_1} \left(2 + \frac{r_1}{r_c} \right) \left(1 - \frac{r_1}{r_c} \right)^2 - \frac{1}{(m_{Ar_c})^2} \right\} \right] \quad (r > r_c). \quad (86)$$

In deriving Eq. (86) we have used the relation $\epsilon_{\text{th}} + [(r_1/r_c)^2 - 1]/2 = r_1/(m_{Ar_c}^2)$ coming from Eq. (51).

For the parameter values $n = 1$, $\rho_A = 1 \text{ g/cm}^3$, $\rho_B = 10^{-4} \text{ g/cm}^3$ and $\Delta r_c/r_c = 0.0625$ used in the numerical simulation of Ref. [13], we obtain $1/(m_{Ar_c}) = 0.0200$ and $\epsilon_{\text{th}} = 0.0793$ from Eqs. (83) and (52). In this case the condition $\Delta r_c/r_c > 1/(m_{Ar_c})$ is satisfied so that the field acquires sufficient kinetic energy in the region $r_1 < r < r_c$. One can also consider the case in which the difference of $\Delta r_c/r_c$ and $1/(m_{Ar_c})$ is larger. For example, with $n = 1$, $\rho_A = 1 \text{ g/cm}^3$, $\rho_B = 2.0 \times 10^{-5} \text{ g/cm}^3$, $\Delta r_c/r_c = 0.08$, one has $1/(m_{Ar_c}) = 0.0142$ and $\epsilon_{\text{th}} = 0.0899$. In Fig. 1 we plot the thin-shell field profile for this latter case by choosing the boundary conditions for φ and $\varphi' \equiv d\varphi/dx$ at $x_i \equiv r_i/r_c = 10^{-5}$, using the analytic solution (84). The numerical solution (a) derived by solving Eqs. (80) and (81) shows fairly good agreement with the analytic solution (b) in the region $r < r_1 = 0.92r_c$. On the other hand the agreement is not very good in the region $r > r_1$, with a 20 % difference at the distance $r = 5r_c$.

Inside the body the following relation holds

$$\varphi(r_1) \simeq 1 + \frac{1}{n+1}, \quad \frac{|V_{,\phi}|}{Q\rho_A} \simeq \frac{1}{\varphi^{n+1}}, \quad (87)$$

which gives $|V_{,\phi}(r_1)|/Q\rho_A \simeq 1/2$. This shows that our analytic estimation does not hold well in the region around $r = r_1$. In particular the neglect of the term $V_{,\phi}$ relative to $Q\rho_A$ in the region $r_1 < r < r_c$ gives rise to an error compared to the numerical simulation including this term. We find that the field value numerically obtained in the region $r_1 < r < r_c$ is smaller than the analytic value given in Eq. (85). This leads to the smaller field derivative $\varphi'(x)$ at the surface of the body ($x = 1$). In the numerical solution presented in Fig. 1 the numerical value of $\varphi'(x = 1)$ is different from its corresponding analytic value by about 18 %. This difference is inherited by the field profile outside the body.

In Fig. 1 we also plot the numerical solution (c) derived by solving the field equation with the approximation $V_{\text{eff},\phi} = m_A^2(\phi - \phi_A)$ for $0 < r < r_1$ and $V_{\text{eff},\phi} = Q\rho_A$ for $r_1 < r < r_c$. We find that the solution (c) agrees well with the analytic solution (b). This shows that the reason for the discrepancy between the solutions (a) and (b) is due to the fact that the matching of two analytic solutions at $r = r_1$ overestimates the field values and their derivatives in the region $r_1 < r < r_c$. We have also tried other model parameters and have found that this property holds generally.

If we take boundary conditions with larger values of $\varphi(x)$ or $\varphi'(x)$ than those estimated by Eq. (84) around the centre of the body, it is possible to obtain a field profile outside the body that is close to the analytic estimation (86). In Fig. 2 we show the numerical solution corresponding to the same model parameters as given in Fig. 1 but with a boundary condition for the field that is larger than the one given by the analytic solution (84). As can be seen in this case the numerical solution outside the body agrees well with the analytic solution (86). Note that the field approaches the asymptotic value $\varphi_B \equiv \phi_B/\phi_A = 223.6$, estimated analytically using the relation $\varphi_B = (\rho_A/\rho_B)^{1/(n+1)}$.

The above results show that the analytic solution is useful to find boundary conditions in order to determine the thin-shell field profile. If we choose the field value to be slightly larger than the one estimated by Eq. (84) around the centre of the body, we are able to find a numerical solution outside the body that is close to the analytic solution (86).

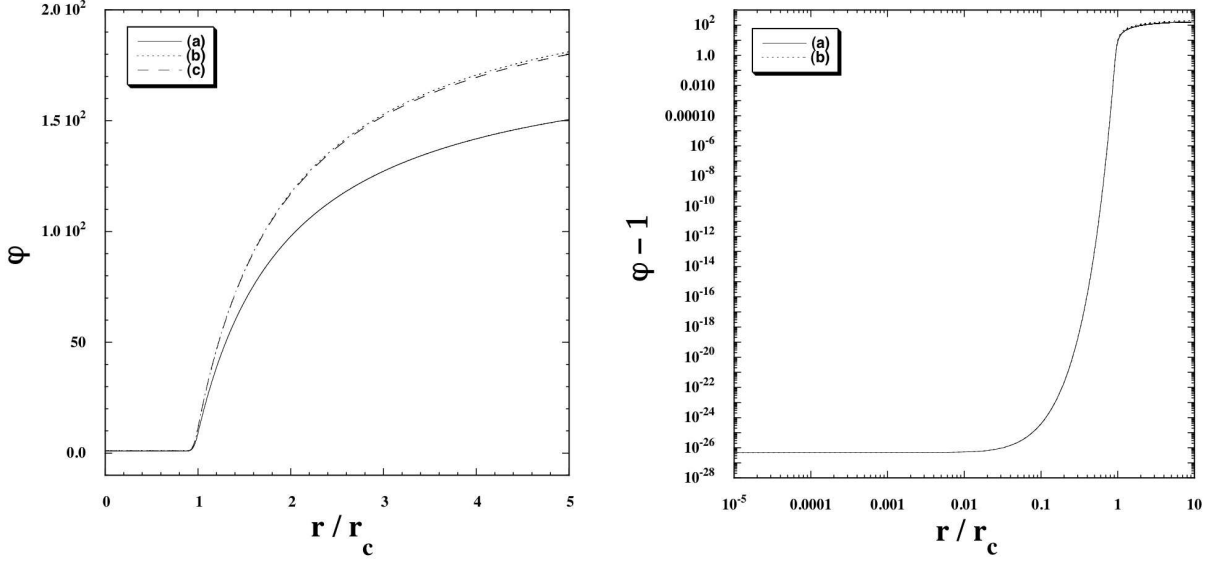


Figure 1: The thin-shell field profile in the Minkowski background for $n = 1$, $Q = 1$, $\rho_A/\rho_B = 5.0 \times 10^4$, and $\Delta r_c/r_c = 0.08$. This case corresponds to $1/(m_A r_c) = 0.0142$ and $\epsilon_{\text{th}} = 0.0899$. The boundary conditions for φ and φ' at $x_i = 10^{-5}$ are chosen by using the analytic solution (84). In the left panel the black curve (a) shows the numerically integrated solution. The dotted curve (b) corresponds to the analytic field profile given in Eqs. (84)-(86). The dashed curve (c) corresponds to the numerical solution that is derived by solving the field equations using the approximations $V_{\text{eff},\phi} = m_A^2(\phi - \phi_A)$ for $0 < r < r_1$ and $V_{\text{eff},\phi} = Q\rho_A$ for $r_1 < r < r_c$. While the curve (c) agrees with the curve (b) with high accuracy, the curve (a) deviates from the curve (b) in the region $r > r_1 = 0.92r_c$. This shows that the analytic estimation that connects two solutions at $r = r_1$ overestimates the field value outside the body (about 20 % larger at the distance $r = 5r_c$ in this case). The right panel is the magnified log plot of $(\varphi - 1)$ in the region $0 < r/r_c < 1.4$. While the numerical solution (a) agrees well with the analytic solution in the region $r < r_1$, the deviation begins to appear in the region $r > r_1$ (in the log plot the deviation appears to be small).

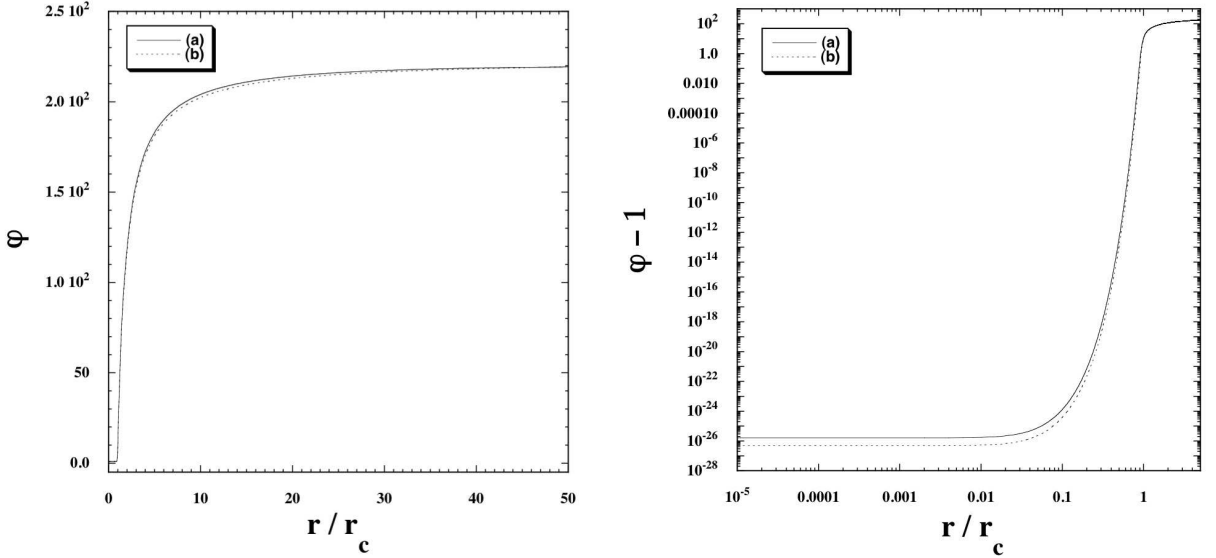


Figure 2: The thin-shell field profile in the Minkowski background for the same model parameters as given in Fig. 1, but with a different boundary condition for φ at $x_i = 10^{-5}$: $\varphi(x_i) - 1 = 1.630 \times 10^{-26}$ (which is larger than the one used in Fig. 1: $\varphi(x_i) - 1 = 4.889 \times 10^{-27}$). The derivative $\varphi'(x)$ at $x = x_i$ is the same as in the case of Fig. 1: $\varphi'(x_i) = 8.074 \times 10^{-29}$. The black curve (a) and the dotted curve (b) show the numerically integrated solution and the analytic field profile, respectively. The left panel is the plot in the region $0 < r/r_c < 50$, whereas the right panel is the magnified log plot of $(\varphi - 1)$ in the region $0 < r/r_c < 5$. In this case the numerical solution approaches the asymptotic field value $\varphi_B = \phi_B/\phi_A = 223.6$ in the limit $r/r_c \rightarrow \infty$. In the region outside the body the analytic solution agrees well with the numerical solution.

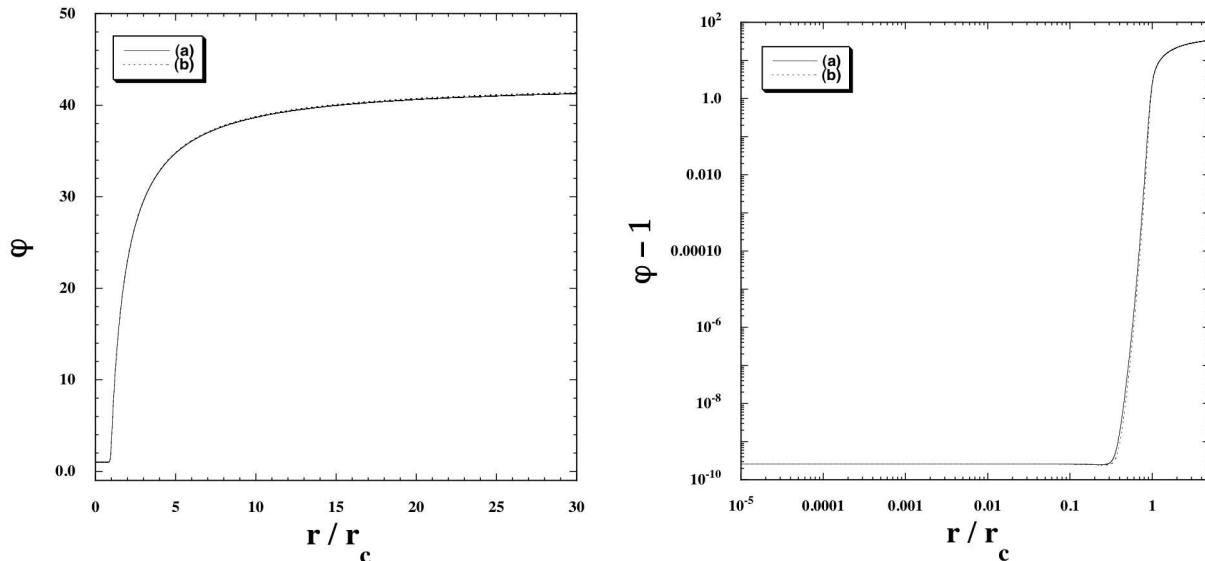


Figure 3: The thin-shell field profile for $\Phi_c = 7.0 \times 10^{-10}$, $n = 3$, $Q = 1$, $\Delta r_c/r_c = 0.085$ and $m_A r_c = 40.0$. This case corresponds to $\rho_A/\rho_B = 3.3 \times 10^6$, $\phi_A = 1.05 \times 10^{-11}$, $\phi_B = 4.48 \times 10^{-10}$ and $\epsilon_{\text{th}} = 0.104$. The boundary condition for the field at $x_i = 10^{-5}$ is $\varphi(x_i) - 1 = 2.615210 \times 10^{-10}$, which is slightly larger than the analytic value $\varphi(x_i) - 1 = 2.615179 \times 10^{-10}$ that comes from Eq. (76). The derivative $\varphi'(x_i)$ is chosen to be the same as the analytic value. The left panel shows φ in the region $0 < r/r_c < 30$, while the right panel depicts $(\varphi - 1)$ in the region $0 < r/r_c < 5$ with log scales in the vertical and horizontal axes. The black curve (a) shows the numerically integrated solution, while the dotted curve (b) is the analytic field profile given in Eqs. (76)-(78). The solution approaches the asymptotic value $\varphi_B = 42.705$.

B. The relativistic gravitational background ($\Phi_c \neq 0$)

We shall proceed to the case of the relativistic gravitational background. As we already explained in Sec. IV, the presence of a relativistic pressure is important around the centre of the body. This relativistic pressure gives rise to a force against the driving force that comes from the slope of the field potential. If the condition (63) is satisfied, the field evolves toward smaller values in the region $0 < r < r_2 = 1/m_A$. In this case the field derivative $\phi'(r)$ needs to change sign at $r = r_3$ ($r_2 < r_3 < r_1$) for the realisation of the thin-shell solution. If $\phi'(r)$ is positive in the region $0 < r < r_1$, the field dynamics is similar to the one in the Minkowski background, discussed in the previous subsection.

Let us now consider the case $\phi'(r) < 0$ in the region $0 < r < r_3$. As long as $m_A r_1 \gg 1$ this situation naturally appears even in weak gravity backgrounds such as in the case of the Earth or the Sun. In Fig. 3 we present an example of a numerically integrated field profile corresponding to the gravitational potential of the Earth with $\Phi_c = 7.0 \times 10^{-10}$ and $n = 3$, $Q = 1$, $\Delta r_c/r_c = 0.085$ and $m_A r_c = 40.0$. We choose the boundary condition of ϕ at $x_i = 10^{-5}$ to be slightly larger than the analytic value derived from Eq. (76), so that the numerical solution approaches the field value $\varphi_B = \phi_B/\phi_A = 42.705$ asymptotically. The reason for this choice is that matching two analytic solutions at $r = r_1$ leads to an overestimation of the field value by neglecting the term V_ϕ relative to the term $Q\rho_A$ in the region $r_1 < r < r_c$. The resulting field profile is sensitive to a slight change of the boundary condition for $\varphi(x_i)$. This shows the importance to derive analytic solutions for finding appropriate thin-shell solutions, as we have done in previous sections.

In the region $0 < r < r_3 \simeq 0.26r_1$ the derivative $\phi'(r)$ is negative. It changes sign at $r = r_3$ and the field begins to grow in the region $r > r_3$ for increasing r . This behaviour is confirmed in the right panel of Fig. 3. Around the surface of the body the field acquires sufficient kinetic energy so that it climbs up the potential hill toward $\phi = \phi_B$. The left panel of Fig. 3 shows that the numerical solution outside the body agrees well with the analytic thin-shell solution given in Eq. (78). Thus the chameleon mechanism is present in the relativistic background with weak gravity ($\Phi_c \ll 1$).

For larger gravitational potential Φ_c , the effect of the relativistic pressure becomes stronger around the centre of the body. This leads to the rapid evolution of the field ϕ toward smaller values. We also note that the analytic thin-shell solution (76)-(78) begins to lose its accuracy in the stronger gravitational backgrounds with $\Phi_c \gtrsim 0.1$. If we run our numerical code by choosing boundary conditions for $\phi(r)$ and $\phi'(r)$ around the centre of the body determined by Eq. (76), the solutions with $\Phi_c \gtrsim 0.1$ typically keep evolving toward smaller ϕ regions by overshooting the effective potential maximum at $\phi = \phi_A$. However, if we choose boundary conditions for ϕ which are larger than the one

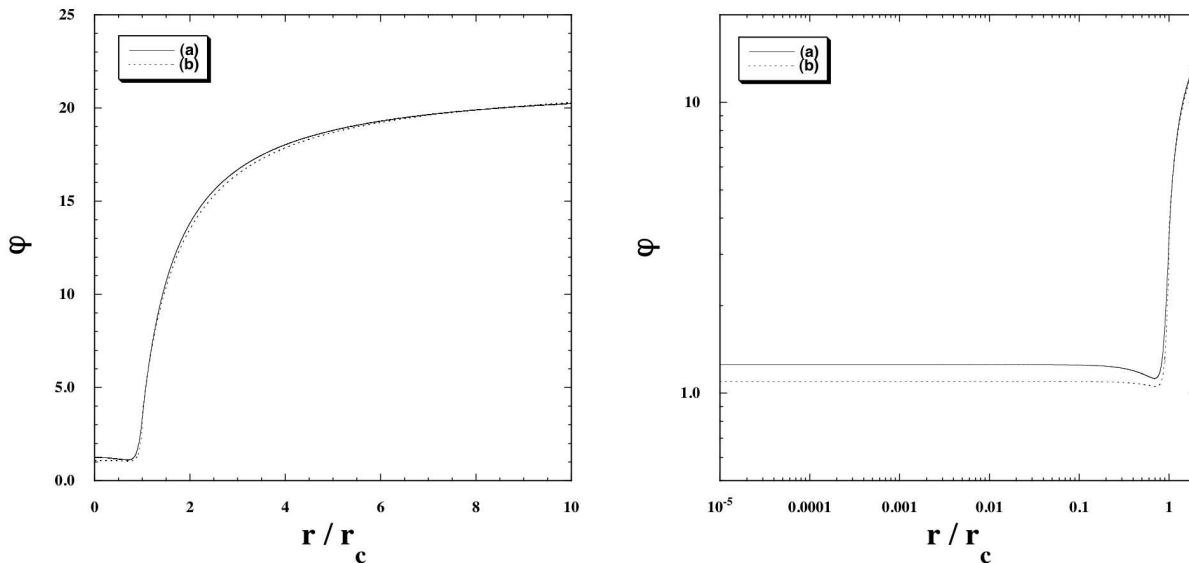


Figure 4: The thin-shell field profile for $\Phi_c = 0.2$, $n = 2$, $Q = 1$, $\Delta r_c/r_c = 0.1$ and $m_A r_c = 20.0$. This case corresponds to $\rho_A/\rho_B = 1.04 \times 10^4$, $\phi_A = 8.99 \times 10^{-3}$, $\phi_B = 1.97 \times 10^{-1}$ and $\epsilon_{\text{th}} = 1.56 \times 10^{-1}$. The boundary condition of the field at $x_i = 10^{-5}$ is $\varphi(x_i) = 1.2539010$, which is larger than the analytic value $\varphi(x_i) = 1.09850009$ that comes from Eq. (76). The derivative $\varphi'(x_i)$ is chosen to be the same as the analytic value. The left panel depicts φ in the region $0 < r/r_c < 10$, while the right panel depicts φ in the region $0 < r/r_c < 2$ with log scales in the vertical and horizontal axes. The black curve (a) and the dotted curve (b) correspond to the numerically integrated solution and the analytic field profile (76)-(78), respectively. The numerical solution outside the body recovers the analytic field profile (78).

given by the corresponding analytic value, we find that it is possible to reproduce the analytic thin-shell solution (78) outside the body even for $\Phi_c \sim 0.1$. The need for the choice of larger ϕ partially comes from the overestimation of the field around $r = r_1$, as was explained above. Moreover, since the pressure is underestimated in our linear expansion of Φ_c , we need to choose values of ϕ larger than the corresponding analytic values in order to prevent the field from entering the region $\phi < \phi_A$.

In Fig. 4 we plot an example of the numerical solution for $\Phi_c = 0.2$, $n = 2$, $Q = 1$, $\Delta r_c/r_c = 0.1$ and $m_A r_c = 20.0$, together with the corresponding analytic field profile. We have used the boundary condition $\varphi(x_i = 10^{-5}) = 1.2539010$, which is larger than the analytic value $\varphi(x_i = 10^{-5}) = 1.09850009$ estimated by Eq. (76). We note again that the resulting field profile is sensitive to the change of boundary conditions. As can be seen from the right panel of Fig. 4 the derivative $\phi'(r)$ is negative in the region $0 < r/r_c < 0.69$. The field grows for increasing r in the region $r/r_c > 0.69$ so that it enters the thin-shell regime for $r/r_c > 0.9$. The left panel of Fig. 4 shows that the numerical solution outside the body agrees well with the corresponding analytical solution. The solution asymptotically approaches the field value $\phi_B/\phi_A = 21.844$.

We have also carried out numerical simulations for other model parameters in the strong gravitational backgrounds. We find that thin-shell solutions are present for $\Phi_c \lesssim 0.3$, which marginally includes the case of neutron stars. When $\Phi_c \gtrsim 0.3$, however, the field continues to evolve toward smaller ϕ and overshoots the effective potential maximum at $\phi = \phi_A$ (i.e., $\varphi = 1$) unless the boundary condition around the centre of the body is chosen to be $\phi/\phi_A \gg 1$. The evolution of the field is typically followed by the rapid roll-down along the potential toward the singularity at $\phi = 0$ (as in the numerical simulations of Kobayashi and Maeda [25] for the $f(R)$ dark energy model of Starobinsky [30]). Since the ratio $p_m(r)/\rho_A$ is of the order of Φ_c around the centre of the body, the pressure force is so strong that the field typically overshoots the effective potential maximum in such cases. We stress here that in strong gravitational backgrounds with $\Phi_c = \mathcal{O}(1)$ a separate analysis is required without recourse to the analytic solutions derived here which are valid only in the regimes with $\Phi_c \lesssim \mathcal{O}(0.1)$.

Finally we note that the distance r_3 at which $\phi'(r_3) = 0$ gets smaller for decreasing m_A (see Table I). This may suggest that it is possible to avoid the overshooting of the field by choosing smaller values of m_A . However, the parameter $\Delta r_c/r_c$ needs to satisfy the conditions $\Delta r_c/r_c \ll 1$ and $\Delta r_c/r_c \gg 1/m_A r_c$. This implies that we can not choose the values of $m_A r_c$ that are smaller than the order of 10. Thus when $\Delta r_c/r_c \lesssim 0.1$ and $m_A r_c \gtrsim 10$, it is typically difficult to obtain thin-shell solutions for $\Phi_c \gtrsim 0.3$, whereas thin-shell solutions are present for $\Phi_c \lesssim 0.3$.

VI. CONCLUSIONS

In this paper we have studied the behaviour of the chameleon scalar field ϕ in the relativistic gravitational background of the spherically symmetric space time. The gravitational potentials Φ and Ψ are found analytically under the conditions that the density of the central compact object is constant and that the energy density of the chameleon field is much smaller than that of the matter. Using the gravitational potential Φ_c at the surface of the body as a linear expansion parameter we have derived the scalar-field equation (17).

The solutions to the field equations can be obtained by considering the perturbation $\delta\phi$ about the corresponding solution ϕ_0 in the Minkowski background. In the region $0 < r < r_1$ the field exists around the minimum of the effective potential $V_{\text{eff}}(\phi) = V(\phi) + Q\rho_A\phi$ inside the body. The thin-shell case corresponds to settings in which r_1 is close to the radius r_c of the body. In the region $r_1 < r < r_c$ the coupling term $Q\rho_A\phi$ dominates over the effective potential, which leads to rapid changes in the field. Using linear expansions in terms of Φ_c and $\delta\phi$ we have derived the solutions of the field equation in the regions $0 < r < r_1$ and $r_1 < r < r_c$, see Eqs. (30) and (33). Outside the body, the kinetic energy of the field dominates over its potential energy, so that the approximate solution in this region is given by Eq. (35).

We have matched the three solutions at the distances r_1 and r_c subject to boundary conditions (26) and have derived the analytical thin-shell field profile given by Eqs. (56)-(58). In discussing the analytical field profile, we have considered the case $Q > 0$ for simplicity. Compared to the result of the Minkowski spacetime, the field ϕ around the centre of the body is shifted due to the presence of a relativistic pressure. For larger values of Φ_c and $m_A r_c$, the field derivative $\phi'(r)$ becomes negative in the region $0 < r < r_3$ ($< r_1$). For values of $r > r_3$, $\phi'(r)$ becomes positive and the field $\phi(r)$ begins to grow with increasing r . As long as the condition $\Delta r_c/r_c \gg 1/(m_A r_c)$ is satisfied, the field acquires sufficient kinetic energy in the thin-shell regime in order to climb up the potential hill outside the body.

For the class of potentials $V(\phi) = M^{4+n}\phi^{-n}$ we have carried out numerical simulations by using the information provided by the analytic field profile in order to set the boundary conditions around the centre of the body. In the Minkowski background ($\Phi_c = 0$) the thin-shell field profile outside the body can be recovered numerically by choosing the boundary condition of the field to be larger than the corresponding analytic value. The reason for this comes from the fact that the analytic solution overestimates the field value in the region $r_1 < r < r_c$ by neglecting the term $V_{,\phi}$ relative to $Q\rho_A$.

In the relativistic gravitational backgrounds with $\Phi_c \lesssim 0.3$ we have also confirmed the presence of thin-shell solutions numerically. While there exists a region in which $\phi'(r)$ is negative inside the body, it is possible to realize thin-shell solutions if the derivative $\phi'(r)$ changes sign at a distance $r = r_3$ smaller than r_1 . For larger Φ_c the distance r_3 tends to increase so that the effect of the relativistic pressure is stronger inside the body. We note that our analysis does not cover the case of extremely strong gravitational backgrounds with Φ_c of the order of unity. This requires a separate detailed analysis which incorporates the formation of black holes.

Finally we note that realistic stars have densities $\rho_A(r)$ that globally decrease as a function of r . It would be expected that this decreasing density may work as a counter term to the relativistic pressure around the centre of the body [see Eq. (11)]. It would be of interest to see whether thin-shell solutions are present in such realistic cases with strong gravitational backgrounds. We shall return to this question in future.

ACKNOWLEDGEMENTS

We thank Justin Khoury, Tsutomu Kobayashi and David Langlois for useful correspondences and discussions. ST thanks financial support for JSPS (No. 30318802). ST is thankful for kind hospitality during his stay at Queen Mary University of London at which this work was initiated.

-
- [1] V. Sahni and A. A. Starobinsky, *Int. J. Mod. Phys. D* **9**, 373 (2000); V. Sahni, *Lect. Notes Phys.* **653**, 141 (2004); S. M. Carroll, *Living Rev. Rel.* **4**, 1 (2001); T. Padmanabhan, *Phys. Rept.* **380**, 235 (2003); P. J. E. Peebles and B. Ratra, *Rev. Mod. Phys.* **75**, 559 (2003); E. J. Copeland, M. Sami and S. Tsujikawa, *Int. J. Mod. Phys. D* **15**, 1753 (2006); S. Nojiri and S. D. Odintsov, *Int. J. Geom. Meth. Mod. Phys.* **4**, 115 (2007); T. P. Sotiriou and V. Faraoni, arXiv:0805.1726 [gr-qc].
 - [2] Y. Fujii, *Phys. Rev. D* **26**, 2580 (1982); L. H. Ford, *Phys. Rev. D* **35**, 2339 (1987); C. Wetterich, *Nucl. Phys. B.* **302**, 668 (1988); B. Ratra and J. Peebles, *Phys. Rev. D* **37**, 321 (1988); R. R. Caldwell, R. Dave and P. J. Steinhardt, *Phys. Rev. Lett.* **80**, 1582 (1998).
 - [3] T. Chiba, T. Okabe and M. Yamaguchi, *Phys. Rev. D* **62**, 023511 (2000); C. Armendariz-Picon, V. F. Mukhanov and P. J. Steinhardt, *Phys. Rev. Lett.* **85**, 4438 (2000).

- [4] A. Sen, JHEP **0204**, 048 (2002); T. Padmanabhan, Phys. Rev. D **66**, 021301 (2002); E. J. Copeland, M. R. Garousi, M. Sami and S. Tsujikawa, Phys. Rev. D **71**, 043003 (2005).
- [5] J. E. Lidsey, D. Wands and E. J. Copeland, Phys. Rept. **337**, 343 (2000); M. Gasperini and G. Veneziano, Phys. Rept. **373**, 1 (2003).
- [6] A. A. Starobinsky, Phys. Lett. B **91**, 99 (1980); S. Capozziello, Int. J. Mod. Phys. D **11**, 483, (2002); S. Capozziello, V. F. Cardone, S. Carloni and A. Troisi, Int. J. Mod. Phys. D, **12**, 1969 (2003); S. M. Carroll, V. Duvvuri, M. Trodden and M. S. Turner, Phys. Rev. D **70**, 043528 (2004); S. Nojiri and S. D. Odintsov, Phys. Rev. D **68**, 123512 (2003).
- [7] L. Amendola, Phys. Rev. D **60**, 043501 (1999); J. P. Uzan, Phys. Rev. D **59**, 123510 (1999); T. Chiba, Phys. Rev. D **60**, 083508 (1999); N. Bartolo and M. Pietroni, Phys. Rev. D **61** 023518 (2000); F. Perrotta, C. Baccigalupi and S. Matarrese, Phys. Rev. D **61**, 023507 (2000); B. Boisseau, G. Esposito-Farese, D. Polarski and A. A. Starobinsky, Phys. Rev. Lett. **85**, 2236 (2000).
- [8] K. i. Maeda, Phys. Rev. D **39**, 3159 (1989).
- [9] C. Brans and R. H. Dicke, Phys. Rev. **124**, 925 (1961).
- [10] S. Tsujikawa, K. Uddin, S. Mizuno, R. Tavakol and J. Yokoyama, Phys. Rev. D **77**, 103009 (2008).
- [11] L. Amendola, Phys. Rev. D **62**, 043511 (2000).
- [12] L. Amendola, D. Polarski and S. Tsujikawa, Phys. Rev. Lett. **98**, 131302 (2007).
- [13] J. Khoury and A. Weltman, Phys. Rev. Lett. **93**, 171104 (2004).
- [14] J. Khoury and A. Weltman, Phys. Rev. D **69**, 044026 (2004).
- [15] B. Ratra and P. J. E. Peebles, Phys. Rev. D **37**, 3406 (1988); I. Zlatev, L. M. Wang and P. J. Steinhardt, Phys. Rev. Lett. **82**, 896 (1999).
- [16] P. Brax, C. van de Bruck, A. C. Davis, J. Khoury and A. Weltman, Phys. Rev. D **70**, 123518 (2004).
- [17] S. S. Gubser and J. Khoury, Phys. Rev. D **70**, 104001 (2004); B. Feldman and A. E. Nelson, JHEP **0608**, 002 (2006).
- [18] A. W. Brookfield, C. van de Bruck and L. M. H. Hall, Phys. Rev. D **74**, 064028 (2006); I. Navarro and K. Van Acoleyen, JCAP **0702**, 022 (2007); I. Navarro, JCAP **0802**, 005 (2008); T. Faulkner, M. Tegmark, E. F. Bunn and Y. Mao, Phys. Rev. D **76**, 063505 (2007); S. Capozziello and S. Tsujikawa, Phys. Rev. D **77**, 107501 (2008); N. Deruelle, M. Sasaki and Y. Sendouda, Phys. Rev. D **77**, 124024 (2008); P. Brax, C. van de Bruck, A. C. Davis and D. J. Shaw, arXiv:0806.3415 [astro-ph].
- [19] T. Clifton, D. F. Mota and J. D. Barrow, Mon. Not. Roy. Astron. Soc. **358**, 601 (2005).
- [20] S. Das and N. Banerjee, Phys. Rev. D **78**, 043512 (2008).
- [21] P. Brax, C. van de Bruck and A. C. Davis, JCAP **0411**, 004 (2004).
- [22] D. F. Mota and D. J. Shaw, Phys. Rev. Lett. **97**, 151102 (2006); Phys. Rev. D **75**, 063501 (2007).
- [23] P. Brax, C. van de Bruck, A. C. Davis, D. F. Mota and D. Shaw, Phys. Rev. D **76**, 085010 (2007); Phys. Rev. D **76**, 124034 (2007); P. Brax, C. van de Bruck and A. C. Davis, Phys. Rev. Lett. **99**, 121103 (2007); M. Ahlers, A. Lindner, A. Ringwald, L. Schrempp and C. Weniger, Phys. Rev. D **77**, 015018 (2008).
- [24] T. Tamaki and S. Tsujikawa, Phys. Rev. D **78**, 084028 (2008).
- [25] T. Kobayashi and K. i. Maeda, Phys. Rev. D **78**, 064019 (2008); Phys. Rev. D **79**, 024009 (2009).
- [26] A. V. Frolov, Phys. Rev. Lett. **101**, 061103 (2008).
- [27] L. Amendola, R. Gannouji, D. Polarski and S. Tsujikawa, Phys. Rev. D **75**, 083504 (2007); L. Amendola and S. Tsujikawa, Phys. Lett. B **660**, 125 (2008).
- [28] B. Li and J. D. Barrow, Phys. Rev. D **75**, 084010 (2007).
- [29] W. Hu and I. Sawicki, Phys. Rev. D **76**, 064004 (2007).
- [30] A. A. Starobinsky, JETP Lett. **86**, 157 (2007).
- [31] S. A. Appleby and R. A. Battye, Phys. Lett. B **654**, 7 (2007).
- [32] S. Tsujikawa, Phys. Rev. D **77**, 023507 (2008).